Droplet impact on a dry surface: triggering the splash with a small obstacle

By C. Josserand[1], L. Lemoyne[2], R. Troeger[2] and S. Zaleski[1]

[1]Laboratoire de Modélisation en Mécanique, case 162, 4 place Jussieu, 75005 Paris, France
[2] Laboratoire de Mécanique Physique, 2 pce. gare de ceinture, 78210 St. Cyr, France,
josseran@lmm.jussieu.fr

(Received 7 April 2004)

Droplet impact on a solid surface is investigated experimentally. A small obstacle made by layers of adhesive tape is located on the solid surface at some distance from the impact center. The splashing of the drop starts at the tape, as a sheet of liquid shoots upwards. Angle, speed and dynamics of this liquid sheet are investigated as a function of the distance from the impact center to the obstacle and its height. Reynolds and Weber numbers are kept constant. Volume of Fluid simulations reproduce the experiments qualitatively. Measured sheet angles are compared with the predictions of a simple theory.

1. Introduction

Splashing, corolla crown formation, and jets are well known features of droplet impacts. Famous photographs (Edgerton & Killian 1954; Worthington 1876) and everyday-life situations have popularized these phenomena. Drop impact, though being an old and almost classical problem, has benefited of numerous recent studies enhanced by both the improvement of vizualisation and experimental techniques and by the tremendious developpment of numerical techniques and power (Stow & Hadfield 1981; Yarin & Weiss 1995; Cossali *et al.* 1997; Gueyffier & Zaleski 1998; Rieber & Frohn 6-8 July 1998; Weiss & Yarin 1999; Bussman *et al.* 2000; **?**; M.R. Davidson 2000; Rioboo *et al.* 2001; S.T. Thoroddsen 2002; Roisman & Tropea 2002; C. Josserand and S. Zaleski 2003). Fluid impacts appear indeed in various contexts, including many technological applications. Examples include ink-jet printing (Chaudhary & Maxworthy 1980; Wallace 2001), sea-wave impacts (M.J. Cooker & D.H. Peregrine 1995), or coating processes (Oğuz & Prosperetti 1990). Splashing and spreading correspond also to a dramatic change in the topological structures of the free-surface flow after impact. Understanding the transition from one to the other is of fundamental importance for our knowledge of such flows (Peregrine 1981; Rein 1993). Consider the simple case of a vertical droplet impact on a horizontal dry solid surface. Depending on the parameters one can observe a large variety of results (Rioboo *et al.* 2001). For instance, low surface tension and low viscosity (large Weber and Reynolds numbers) promote splash, secondary droplets break-up and/or corolla formation. On the other hand, a high viscosity (low Reynolds number) can suppress the splash and only droplet deposition is observed. Similarly, the solid-surface properties have an effect on the formation of splashes. In particular, experiments have shown that the rougher the solid, the easier the droplet splashes (Rioboo *et al.* 2001). The investigation of this as yet unexplained effect motivated the present work. Spreading is sought for good ink-jet printing but splashes are desirable in combustion chambers for instance. Thus, the understanding and control of this splashing/spreading transition are needed both from a fundamental

and a practical point of view. When only capillarity and viscosity are considered, experimental laws have been obtained for both dry and wet surfaces (Mundo *et al.* 1995). They involve the dimensionless splashing parameter $K = \mathrm{We}^{1/2}\mathrm{Re}^{1/4}$. The critical value K_c that separates spreading from splashing behavior depends on other experimental parameters. For impacts on thin liquid films (Yarin & Weiss 1995; C. Josserand and S. Zaleski 2003) K_c depends on the dimensionless ratio between the droplet radius and the liquid layer thickness. For impacts on dry surfaces (Rioboo *et al.* 2001) K_c depends on the surface roughness.

The present study is an attempt to understand this effect through a model experiment. We describe indeed the impact of a droplet on a smooth solid surface with a single, step change of the surface elevation. This localized surface fluctuation forms an obstacle which deviates the rapidly spreading liquid layer. In this first approach, we focus on the phenomenological description of the dynamics since we restrict our presentation to a single choice of Reynolds and Weber numbers. Few numerical and experimental studies have recently been devoted to drop impact on non-flat surfaces in the context on molten droplet impingement (H. Liu, E.J. Lavernia and R.H. Rangel 1995; R. Ghafouri-Azar, S. Shakeri, S. Chandra and J. Mostaghimi 2003) or already to exhibit a modelization of surface roughness (K. Range and F. Feuillebois 1998). For molten droplets impingement, the surface fluctuation is created by the preceeding impacting droplet. Although we observe similar splashing figures thanR. Ghafouri-Azar, S. Shakeri, S. Chandra and J. Mostaghimi (2003), the dynamics for molten droplets is more complex to analyse since the obstacle geometry is not controlled at all, saying nothing on the temperature field and phase transition influences. On the other studies the surface fluctuations were well controlled, either by the addition of grooves on the flat surface (K. Range and F. Feuillebois 1998) or by considering numerical simulations of drop impact on periodically perturbed surfaces(H. Liu, E.J. Lavernia and R.H. Rangel 1995).

2. Experimental setup

Images of impacting droplets are obtained with a classical droplet generator and experimental facility. Experiments are performed with demineralised water. Droplets fall from a precision syringe with a diameter $D = 3.7$mm and impact a plate at speed $U = 3.3$ m/s. The Reynolds $\mathrm{Re} = UD/\nu = 12200$ and Weber number $\mathrm{We} = \rho U^2 D/\sigma = 514$ are fixed throughout the experiments. Droplets prior to impingement were observed and sphericity verified (diameter distorsion is les than 10%).

The plate is inox coated with Teflon in order to avoid wetting as much as possible. An obstacle is set in the course of the spreading droplet by one or several layers of adhesive tape. The height of the obstacle is controlled by the number of layers and the distance between the obstacle and the impact point is measured by a micrometer table. Each layer of tape is 0.035 ± 0.002 mm thick and is placed orthogonally to the observation plane. Obstacle is therefore non axi-symmetrical. The impact plate offers a very smooth surface ($\mathrm{Ra} < 0.5\mu$m, measured before Teflon coating) and its temperature is controlled at 25°C. Pictures are obtained with a Stanford Optics intensified CCD camera triggered by a light barrier consisting of a laser diode opposite a photomultiplier. This solution has been retained in order to obtain maximum repeatability of camera triggering. The triggering is adjusted on the decreasing rate of the photomultiplier signal. Backlighting is realized with a Spectra Physics 355nm Argon laser at 300mW diffused by an acid-polished glass. A specific micro-telescope is mounted on the camera allowing to observe a 1cm-large area. In order to observe small-scale features of the splashing on an obstacle, time exposure has been lowered to 2μs. Different steps of the impingement process are

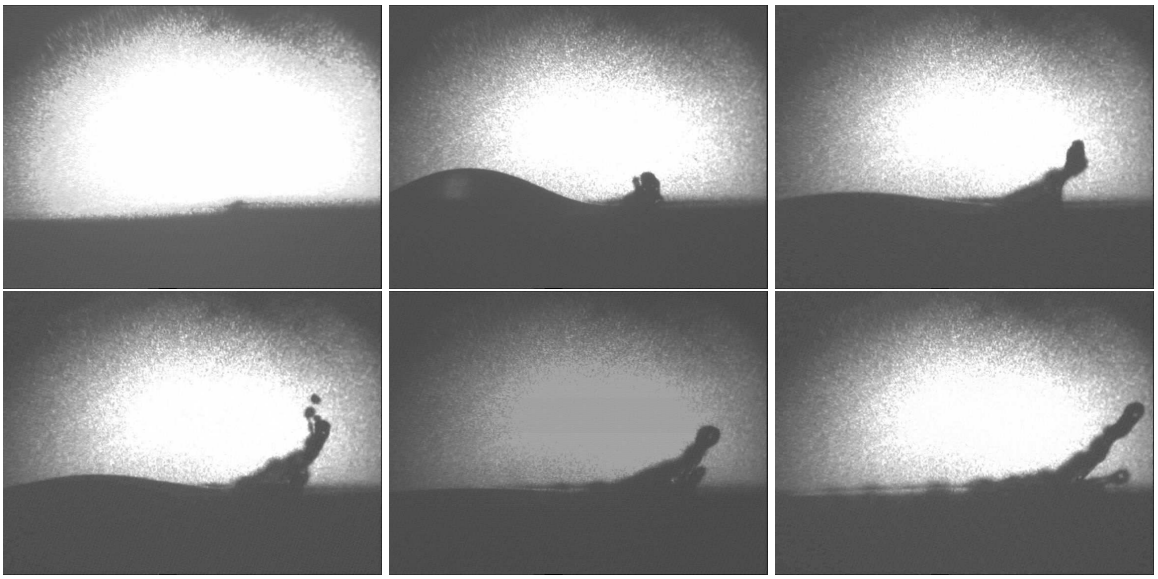

FIGURE 1. Impact on the 0.035mm obstacle (from left to right and top to bottom : void, 1000ms, 1250ms, 1500ms, 2000 ms and 2500 ms)

obtained by controlling the delay of camera triggering with the photomultiplier gate. Velocity measurements during impact are verified by multi-exposure images (not shown here). Repeatability of the overall imaging procedure is improved by manually eliminating obviously failed images, mostly due to parasite light triggering the photomultiplier. Considering different error sources, we estimate the error made on diameter and velocity measurements at 2%, whereas the error made on other values (such as angles and liquid thicknesses) is 5%. The dissertation of Rioboo (2001) gives detailed error estimates for a very similar experimental setup. Although repeatability has been a permanent concern in developing the experimental setup, each time step of impingement is repeated untill three almost identical features are obtained.

3. Results and discussion

Three series of impacts with an obstacle are shown for varying obstacle thicknesses, 0.035 mm , 0.07 mm and 0.2 mm. The distance r between the impact point of the droplet and the obstacle has been varied, from 0 to 4.5mm. In Figures 1 to 3, different stages of impact and splashing are shown.

Figure 1 pictures a droplet falling on a plate with a 0.035mm-high obstacle placed 2mm from the droplet impact center. Figure 2 shows a droplet falling on a plate with an obstacle 0.07mm high placed closer to the center. Last, Figure 3 shows a droplet falling on a plate with an obstacle 0.2mm high at a similar distance than the previous one. Time $t = 0$ is when the droplet touches the plate (not the obstacle).

The onset of a splash when the droplet arrives on the obstacle is clearly seen in these figures. Angle, width and velocity of the liquid sheet that shoots up upon impact vary with the distance from the impact center to the obstacle and the height of the obstacle. Figures 1, 2 and 3 also indicate that the higher the obstacle, the more vertical the liquid sheet will be. Moreover in Figure 4, sheet angles are plotted against time. In a first phase of the interaction of the jet with the obstacle the liquid is ejected almost vertically.

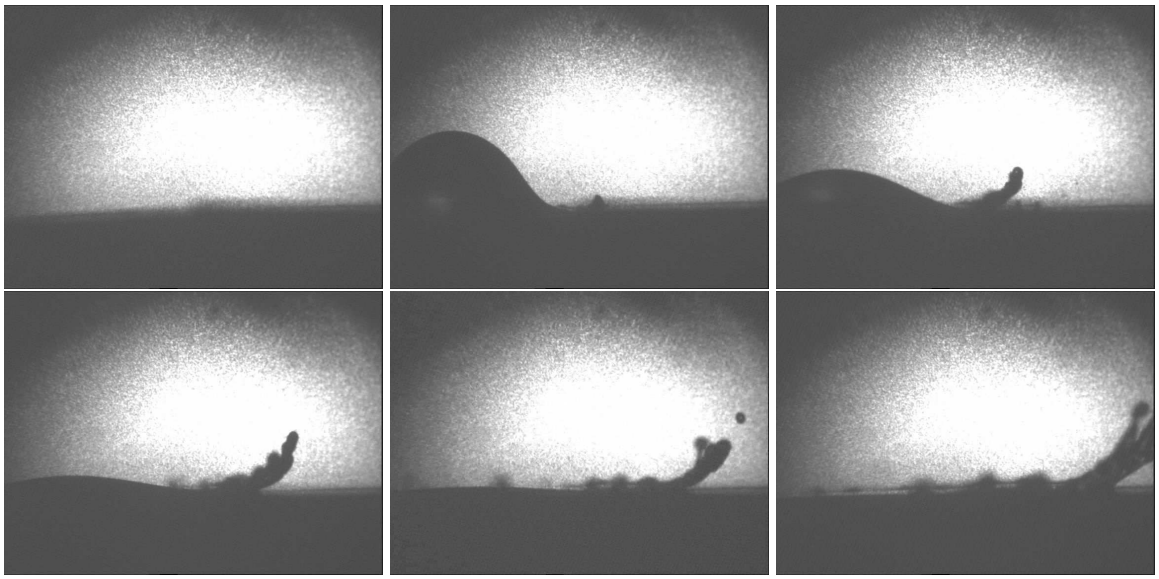

FIGURE 2. Impact on the 0.07mm obstacle (from left to right and top to bottom : void, 500ms, 1000ms, 1500ms, 2000 ms, 2500 ms)

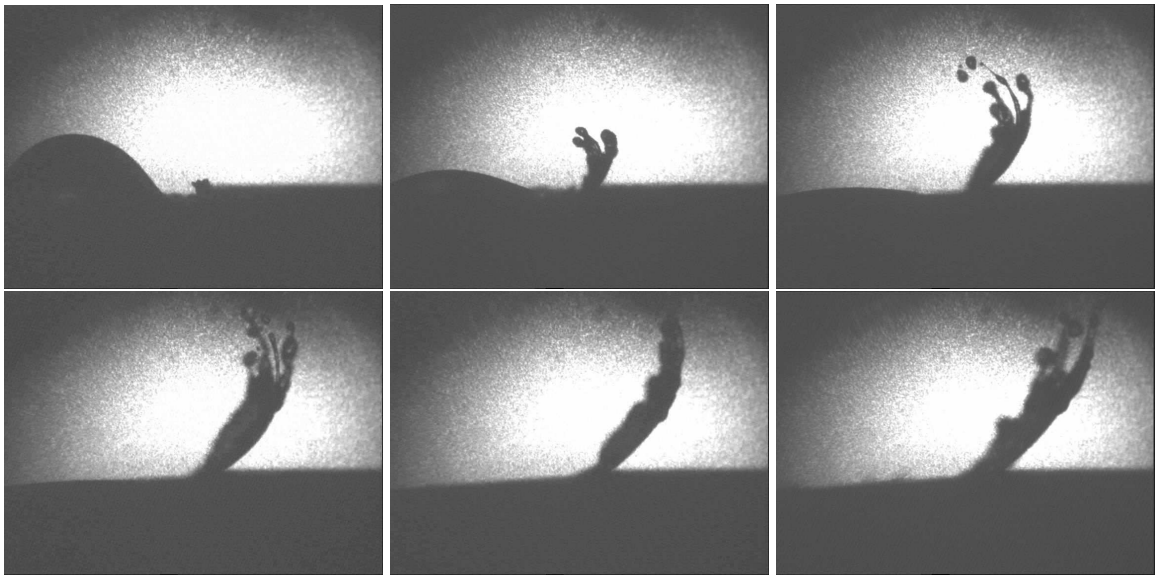

FIGURE 3. Impact on the 0.2mm obstacle (from left to right and top to bottom : 500ms, 1000ms, 1500ms, 2000 ms, 2500 ms and 3000ms)

The liquid sheet fed by the spreading film develops afterwards as the deviation angle decreases, apparently asymptoting a steady state.

In Figure 5 this stabilized apparent angle of the liquid sheet is plotted against the dimensionless (by droplet diameter) obstacle position for a 0.07mm-thick layer. Angle plotted is the angle of the median straight line of liquid sheet and the obstacle plate. When the droplet falls directly on the obstacle (distance of droplet impact point to obstacle is less than dropet radius) no splash is observed (angle 0°). When the splash

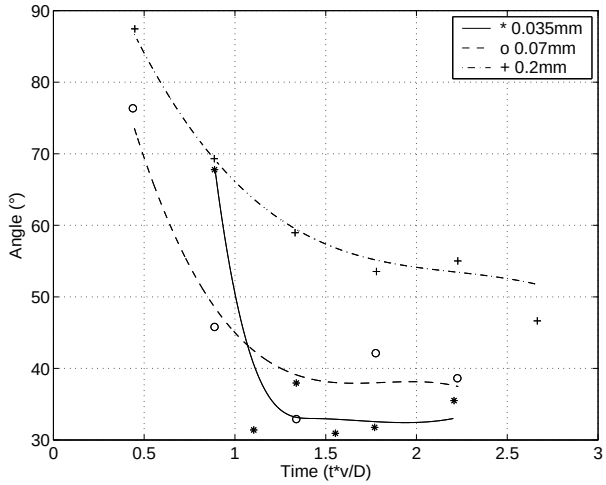

FIGURE 4. Angle of liquid sheet versus dimensionless time. (Symbols represent actual experimental measures, lines represent interpolation of experimental results)

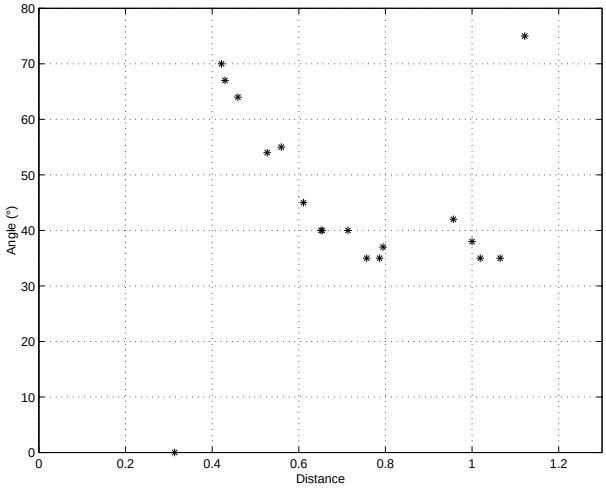

FIGURE 5. Angle of liquid finger versus the dimensionless obstacle distance. Symbols are experimental values and the continous line is the theoretical prediction.

occcurs, the direction of the liquid sheet is the more vertical when the impact is closer to the obstacle. In fact, if an encounter with the obstacle happens in the early stages of spreading, the liquid film seems to be projected vertically, whereas when the obstacle is met at the end of spreading, the liquid film only climbs over the obstacle. This may result from different thicknesses of the liquid film at different stages of spreading confirming a theoretical prediction made by C. Josserand and S. Zaleski (2003) and discussed in section 5 below, that the film gets thicker as time advances. This is a rather difficult fact to verify experimentally with an acceptable precision.

Liquid sheet length can be measured as the distance from the obstacle position to the point where fllaments appear at the upper end (Figure 6). Its evolution with time shows that the liquid sheet has an almost-constant velocity. This interesting feature may be explained as follows. First, when the film is ejected from the droplet theory predicts that this happens at a constant velocity (C. Josserand and S. Zaleski 2003). Second, after

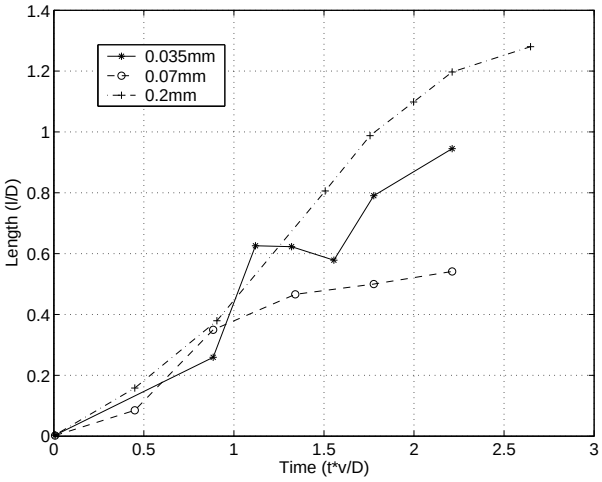

FIGURE 6. Dimensionless length of the liquid sheet versus dimensionless time.

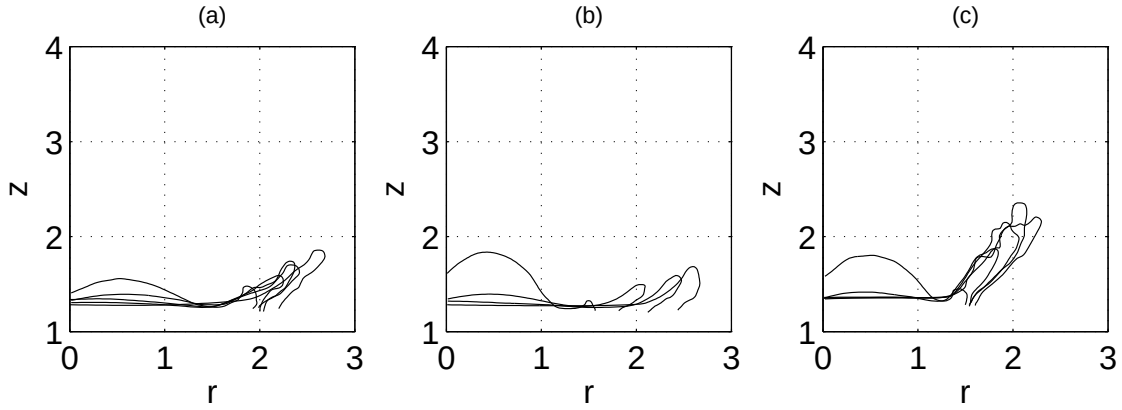

FIGURE 7. Droplet contours at various times. Distances are made dimensionless by droplet diameter.

ejection the velocity is mostly conserved: indeed, we use Teflon-coated plates, which are non-wetting. Thus, the singular viscous dissipation near the contact line is avoided. With little dissipation, the velocity remains constant. Moreover we have observed that the sheet thickness remains roughly constant throughout the explored time span, at around 0.5mm for obstacles of height 0.035mm and 0.07mm, and at 0.7mm for the 0.2mm obstacle.

Secondary droplet formation is enhanced by short distances from the obstacle as less momentum is dissipated between impact with plate and contact with obstacle. Also large obstacles enhance secondary droplet formation. When plotting (Figure 7) on the same image the droplet contours during impact, we observe that with the smaller obstacle (a), the sheet develops to a length higher than with medium size obstacle(b). One may notice also the difference between the center figure (b) (0.07mm obstacle) and the left and right figures (0.035 and 0.2 mm): the base of the sheet seems fixed for 0.035 and 0.2 mm cases whereas it advances over the obstacle with finger development for the 0.07mm case.

4. Numerical simulation

We compare now the dynamics observed in the experiments with numerical simulations of axisymetrical drop impacts. We use here a Volume of Fluid (VOF) numerical scheme already used by two of us for the study of droplet impacts on thin liquid layers (C. Josserand and S. Zaleski 2003).

The main additional difficulties to model drop impact on solid surface arise at the moving contact line. This contact line is located at the frontier between gas, liquid and solid. It still poses a hard challenge for theory and modelling (P.G. de Gennes 1985). In particular, the equations of hydrodynamics lead to a stress singularity near the moving contact line (E.B. Dussan and S.H. Davis 1974). This mathematical singularity can be avoided through still-debated physical cut-off prescriptions (P.G. de Gennes 1985; A. Oron, S.H. Davis and S.G. Bankoff 1997) but researchers lack as yet a full understanding of the dynamics there.

For numerical simulations, a major concern is to suppress this unphysical singularity. The few numerical simulations that have been reported in the literature use various effective cut-offs near the contact line (M. Pasandideh-Fard, Y.M. Qiao, S. Chandra and J. Mostaghimi 1996; Bussman *et al.* 2000; M. Bussmann, S. Chandra and J. Mostaghimi 2000; **?**), but mostly involve a wall-slip condition, which suppresses in particular the moving contact line singularity.

We solve the Navier-Stokes equation for axisymmetric incompressible flow with surface tension written in the one-fluid formulation

$$\rho(\frac{\partial \mathbf{u}}{\partial t} + \mathbf{u} \cdot \nabla \mathbf{u}) = -\nabla p + \mu \Delta \mathbf{u} + \sigma \kappa \delta_s, \mathbf{n} \tag{4.1}$$

where $\mathbf{u}$ is the fluid velocity, ρ the fluid density and p the pressure. The vector $\mathbf{n}$ denotes the normal to the interface, σ is the surface tension and δ_s the delta function restricted to the interface. Gravity is neglected and the continuity equation reads

$$\nabla \cdot \mathbf{u} = 0. \tag{4.2}$$

The discretization is performed on a Marker and Cell (MAC) grid and pressure is solved by the explicit projection method making use of multigrid convergence. The interface is followed by the Volume of Fluid/Piecewise Linear Interface Calculation (VOF/PLIC) method of Li (1995) and the capillary force is computed through a variant of the continuous surface stress and continuous surface force methods (Lafaurie *et al.* 1994; Scardovelli & Zaleski 1999; Gueyffier *et al.* 1999) adapted to axisymmetric geometry. A full description of the method can be found in (Gueyffier *et al.* 1999) except for the adaptation to axisymmetric geometry which is described in (Gueyffier 2000).

The additional layer is made circular here for numerical convenience (axisymmetry) while experiments were made with straight adhesive tape. Boundary conditions are crucial for the modelling. On the solid wall $\mathbf{u} = 0$, and Neuman conditions are taken for the color function: the derivative in the direction normal to the solid vanishes, i.e. $\frac{\partial c}{\partial n} = 0$. This boundary condition imposes a constant contact angle of 90° which corresponds to intermediate wetting. Surprisingly, we have observed numerically that this boundary condition coupled with the no-slip condition results in no singular viscous dissipation near the moving contact line. The numerical discretization acts here as a sufficient cut-off.

These conditions are now applied for all the solid boundaries including the obstacle. However to simplify the writing of the code, the $\mathbf{u} \cdot \mathbf{n} = 0$ boundary condition is not applied during the projection step, i.e. the Poisson equation for the pressure is solved with a flat boundary instead of the obstacle. The pressure field is thus not accurately

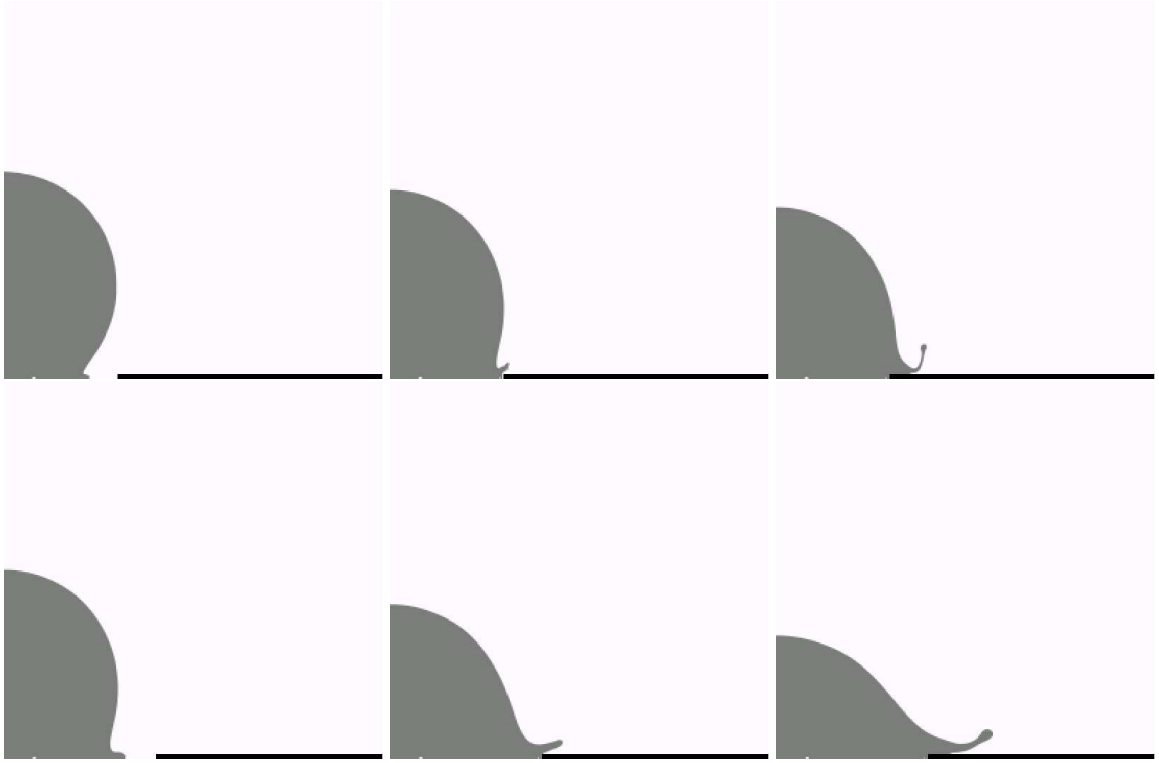

FIGURE 8. Numerical simulation of droplet impact for two distances of the obstacle from the impact center, We = 460 and Re = 540. Top: $r = 0.5D$ and figures show density profiles at times 100, 200 and 300μs. Bottom $r = 0.67D$ and times are respectively 200, 400 and 600μs.

solved near the obstacle. Local mass conservation may not be satisfied: there is a mass flow accross the obstacle. In the simulations reported below the mass loss during the runs is less than 5%.

These numerical simplifications have made quantitative comparisons between experiments and numerics hard to obtain. For instance, for fluid parameters (densities, viscosities, surface tension) similar to the experimental values, the thickness of the spreading film was found much thiner than in experiments. Such discrepancy, probably due to the absence of roughness at the idealized wall surface, leads to a strongly different dynamics since the liquid sheet splashes promptly at the obstacle and breaks up into tiny droplets. To avoid this effect and to increase the numerical film thickness, we have used higher numerical viscosities. Moreover, the gas density was taken twice higher than air density in order to diminushe numerical instabilities due to high density ratio. Following these restrictions, figure (8) shows numerical simulations of impacts for two different distances of the obstacle to the impact center $r = 0.5D$ and $r = 0.67D$. Fluid parameters are as in the experiments but with a higher viscosity to improve numerical stability, so that We = 514 and Re = 2400. There are 256×256 grid points. The obstacle thickness is 0.07 mm to be compared with the drop radius $D/2 = 3.6$ mm. Using this simplified numerical model, we retrieve many features of the experiments. Splashing appears at the obstacle and generates a deviated liquid sheet. The deviation of the liquid is initially almost vertical, then converges to an almost constant angle. Finally, increasing the obstacle distance decreases the liquid deviation as observed experimentally.

5. Theory

We want to study the jet-obstacle interaction in a simplified framework and so consider two-dimensional geometry. We explore the steady flow of a jet of height h, speed U along an horizontal surface encountering a step change e of the surface elevation and thus deviated by an angle θ from the horizontal axis. For inviscid flow without surface tension an exact solution is obtained through complex analysis Birkhoff & Zarantonello (1957). This solution gives the relation between the deviation angle α and the relative obstacle height e/h:

$$\frac{e}{h} = 2(1-\cos\alpha) - \frac{4}{\pi}\sin\alpha \ln[\tan(\frac{\pi}{4} - \frac{\alpha}{2})]. \tag{5.1}$$

We have compared this prediction to computations of this simplified problem using our code. The results which will be published elsewhere are in qualitative agreement for small to moderate α and e/h, up to a proportionality constant C'. Going back to the full problem, we identify h with the thickness of the rapidly expanding film, which is difficult to determine. However a simple estimate can be made as follows. It has been argued by two of us C. Josserand and S. Zaleski (2003) that the thickness of the jet was of the order $h \simeq C\sqrt{\nu t}$ where t is the time from drop impact, and C is a dimensionless constant. Estimating t as the inertial time $t \sim r/U$ (where r is the distance of the step from the impact center) we get

$$h \simeq C\sqrt{\nu r/U}. \tag{5.2}$$

We fix $C = 2$ and obtain from (5.2) and (5.1) the solid line in Figure 6. The general trend is in agreement with the experiment but there is obviously room for improvement: more refined estimates for h could be made.

To summarize, we have observed the triggering of the splash by a small obstacle. Numerical simulations are in qualitative agreement. A simple potential flow model reproduces the trend observed in the experiments. More refined studies, both experimental and theoretical are needed to determine the thickness of the spreading layer. The present study could also be expanded to investigate splashes on a rough surface, modelling the roughness as a collection of small obstacles.

REFERENCES

A. Oron, S.H. Davis and S.G. Bankoff 1997 Long-scale evolution of thin liquid films. *Rev. Mod. Phys.* **69**, 931.

Birkhoff, G. & Zarantonello, E. 1957 *Jets, wakes and cavities*. Academic Press inc.

Bussman, M., S., C. & Mostaghimi, J. 2000 Modeling the splash of a droplet impacting a solid surface. *Phys. Fluids* **12**, 3121.

C. Josserand and S. Zaleski 2003 Droplet splashing on a thin liquid film. *Phys. Fluids* **15**, 1650.

Chaudhary, K. C. & Maxworthy, T. 1980 The nonlinear capillary instability of a liquid jet. part3. experiments on satellite drop formation and control. *J. Fluid Mech.* **96**, 287–297.

Cossali, G., Coghe, A. & Marengo, M. 1997 The impact of a single drop on a wetted solid surface. *Exps. Fluids* **22**, 463–472.

E.B. Dussan and S.H. Davis 1974 On the motion of a fluid-fluid interface along a solid surface. *J. Fluid Mech.* **65**, 71–95.

Edgerton, H. & Killian, J. 1954 *Flash*. Boston: Branford.

Gueyffier, D. 2000 Etude de l'impact de gouttes sur un film liquide mince. PhD thesis, Université Pierre et Marie Curie.

Gueyffier, D., Nadim, A., Li, J., Scardovelli, R. & Zaleski, S. 1999 Volume of fluid interface tracking with smoothed surface stress methods for three-dimensional flows. *J. Comput. Phys.* **152**, 423–456.

Gueyffier, D. & Zaleski, S. 1998 Formation de digitations lors de l'impact d'une goutte sur un film liquide. *C. R. Acad. Sci. IIb* **326**, 839–844.

H. Liu, E.J. Lavernia and R.H. Rangel 1995 Modeling of molten droplet impingement on a non-flat surface. *Acta Metall. Mater.* **43**, pp 2053–2072.

K. Range and F. Feuillebois 1998 Influence of surface roughness on liquid drop impact. *J. Colloid. and Interface Science* **203**, pp 16–30.

Lafaurie, B., Nardone, C., Scardovelli, R., Zaleski, S. & Zanetti, G. 1994 Modelling merging and fragmentation in multiphase flows with SURFER. *J. Comput. Phys.* **113**, 134–147.

Li, J. 1995 Calcul d'interface affine par morceaux (piecewise linear interface calculation). *C. R. Acad. Sci. Paris, série IIb, (Paris)* **320**, 391–396.

M. Bussmann, S. Chandra and J. Mostaghimi 2000 Modeling the splash of a droplet impacting a solid surface. *Phys. Fluids* **12**, 3121.

M. Pasandideh-Fard, Y.M. Qiao, S. Chandra and J. Mostaghimi 1996 Capillary effects during droplet impact on a solid surface. *Phys. Fluids* **8**, 650.

M.J. Cooker & D.H. Peregrine 1995 Pressure-impulse theory for liquid impact problems. *J. Fluid Mech.* **297**, 193–214.

M.R. Davidson 2000 Boundary integral prediction of the spreading of an inviscid drop impacting on a solid surface. *Chem. Eng. Sci.* **55(6)**, 1159.

Mundo, C., Sommerfeld, M. & Tropea, C. 1995 Droplet-wall collisions: Experimental studies of the deformation and breakup process. *Int. J. Multiphase Flow* **21**, 151.

Oğuz, H. & Prosperetti, A. 1990 Bubble entrainment by the impact of drops on liquid surfaces. *J. Fluid Mech.* **219**, 143–179.

Peregrine, D. 1981 The fascination of fluid mechanics. *J. Fluid Mech.* **106**, 59–80.

P.G. de Gennes 1985 Wetting: statics and dynamics. *Rev. Mod. Phys.* **57**, 827.

R. Ghafouri-Azar, S. Shakeri, S. Chandra and J. Mostaghimi 2003 Interaction between molten metal droplets impinging on a solid surface. *Int. J. Heat Mass Transf.* **46**, pp 1395–1407.

Rein, M. 1993 Phenomena of liquid drop impact on solid and liquid surfaces. *Fluid Dyn. Res.* **12**, 61.

Rieber, M. & Frohn, A. 6-8 July 1998 Numerical simulation of splashing drops. Academic Press, proceedings of ILASS98, Manchester.

Rioboo, R. 2001 Impact de gouttes sur surfaces solides et seches. PhD thesis, UPMC Paris6.

Rioboo, R., Marengo, M. & Tropea, C. 2001 Outcomes from a drop impact on solid surfaces. *Atomization and Sprays* **11**, 155–165.

Roisman, I. V. & Tropea, C. 2002 Impact of a drop onto a wetted wall: description of crown formation and propagation. *J. Fluid Mech.* **472**, 373.

Scardovelli, R. & Zaleski, S. 1999 Direct numerical simulation of free-surface and interfacial flow. *Annu. Rev. Fluid Mech.* **31**, 567–603.

S.T. Thoroddsen 2002 The ejecta sheet generated by the impact of a drop. *J. Fluid Mech.* **451**, 373.

Stow, C. & Hadfield, M. 1981 An experimental investigation of fluid flow resulting from the impact of a water drop with an unyielding dry surface. *Proc. R. Soc. London, Ser. A* **373**, 419.

Wallace, D. B. 2001 Ink-jet applications, physics, and modelling - an industrial/applied research view. In *talk delivered at IMA "Hot Topics" Workshop: Analysis and Modeling of Industrial Jetting Processes, http://www.ima.umn.edu/multimedia/abstract/1-10abs.html#wallace.*

Weiss, D. & Yarin, A. 1999 Single drop impact onto liquid films: neck distortion, jetting, tiny bubble entrainment, and crown formation. *J. Fluid Mech.* **385**, 229–254.

Worthington, A. 1876 On the form assumed by drops of liquids falling vertically on a horizontal plate. *Proc. R. Soc. Lond.* **25**, 261–271.

Yarin, A. & Weiss, D. 1995 Impact of drops on solid surfaces: self-similar capillary waves, and splashing as a new type of kinematic discontinuity. *J. Fluid Mech.* **283**, 141–173.